AD-A160 662 AERODYNAMICS OF TWO-DIMENSIONAL BLADE-VORTEX INTERACTION(U) JAI ASSOCIATES MOUNTAIN VIEW CA G R SRINIVASAN ET AL 1985 DAAG29-85-C-0002 1/1

UNCLASSIFIED F/G 1/3 NL

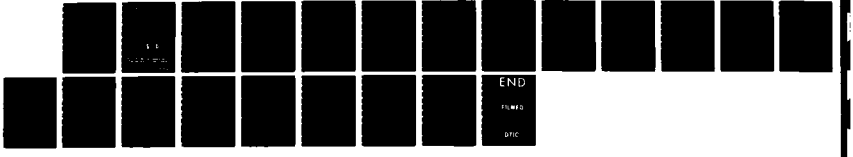

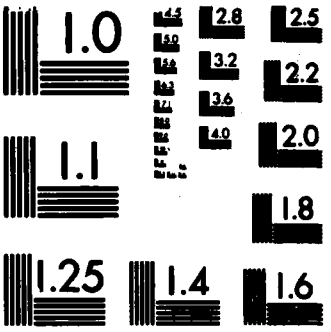

MICROCOPY RESOLUTION TEST CHART
NATIONAL BUREAU OF STANDARDS-1963-A

AIAA'85

AD-A160 662

AIAA-85-1560

Aerodynamics of Two-Dimensional Blade-Vortex Interaction

G.R. Srinivasan
JAI Associates, Mountain View, California
W.J. McCroskey and J.D. Baeder
U.S. Army Aviation Research and Technology Activity-AVSCOM
NASA-Ames Research Center, Moffett Field, California

DTIC COPY INSPECTED

Accesion For
NTIS CRA&I ☒
DTIC TAB ☐
Unannounced ☐
Justification
By
Distribution /
Availability Codes
Dist | Avail and / or Special
A-1

DTIC ELECTE S OCT 23 1985 D A

This document has been approved for public release and sale; its distribution is unlimited.

DTIC FILE COPY

AIAA 18th Fluid Dynamics and Plasmadynamics and Lasers Conference
July 16-18, 1985 / Cincinatti Ohio

85 10 23 010

AERODYNAMICS OF TWO-DIMENSIONAL BLADE-VORTEX INTERACTION

G. R. Srinivasan*
JAI Associates, Mountain View, California

W. J. McCroskey† and J. D. Baeder‡
U.S. Army Aviation Research and Technology Activity-AVSCOM
NASA Ames Research Center, Moffett Field, California

Abstract

A computational procedure and some numerical results of unsteady interaction of a helicopter rotor blade with a Lamb-like vortex of finite viscous core in subsonic and transonic flows is presented. The interaction considered here is one of the limiting cases of a more complex interaction typically encountered on a helicopter rotor blade. In this limit, the interacting flow field is considered to be unsteady but two-dimensional. Accordingly, unsteady, two-dimensional, thin-layer Navier-Stokes equations are solved using a prescribed-vortex method (also called perturbation method) for the cases of stationary and moving rotor blades encountering a moving vortex passing the blades. The numerical results are compared with the recent experimental data of Caradonna et al. for the latter case. The comparison shows that for the transonic cases, the flow field is dominated by the presence of the shock waves, with strong indications of unsteady time lags in the shock-wave motions and shock-wave strengths, and of important three-dimensional effects. For subcritical-flow cases, however, the unsteady lag effects on the basic rotor blade are absent, and three-dimensional effects appear to be negligible, unlike the supercritical case. The subcritical calculations are in good agreement with the experimental data. The presence of three-dimensional influence in the supercritical-flow case is demonstrated by making calculations with a small-disturbance code, after including in it the necessary cross-flow terms. This modification to the two-dimensional, transonic small-disturbance formulation to produce the three-dimensional influence clearly demonstrated the presence of such effects, and these numerical results are in good qualitative agreement with the experimental data. A similar calculation done for the subcritical-flow condition showed almost no three-dimensional influence, suggesting that the three-dimensional influence, if any, seems to be accentuated in the presence of shock waves. In all these calculations, the details of the vortex structure were found to be very important in matching the experimental data.

Nomenclature

A,B,C_1,C_2,D,E	= coefficients as shown in Eq. (10)
$\hat{A},\hat{B}$	= Jacobian matrices
a_o	= vortex core radius
a_{ow}	= a_o/C_w
a_∞	= free-stream sound speed
B1	= $F'(z)/F(z)$; see Appendix
C	= characteristic length scale, chord of the rotor blade
C_L	= lift coefficient
C_M	= quarter-chord pitching-moment coefficient
C_p	= Coefficient of pressure
C_w	= chord of the vortex generating wing
$\hat{E},\hat{E}_o$	= flux vectors
e	= total energy per unit volume
$\hat{F},\hat{F}_o$	= flux vectors
I	= identity matrix
J	= transformation Jacobian
$\hat{M}$	= Jacobian matrix of viscous stress flux vector
M_ℓ	= local Mach number
M_r	= blade reference Mach number ($\Omega r_B/a_\infty$)
M_T	= blade tip Mach number
M_∞	= free-stream Mach number
p	= static pressure
$\hat{Q}$	= velocity induced by the vortex, $\hat{i}u_v + \hat{j}v_v$
$\hat{q}$	= unknown flow-field vector

*Senior Research Scientist. Member AIAA.
†Senior Staff Scientist, Aeroflightdynamics Directorate. Associate Fellow AIAA.
‡Research Scientist, Aeroflightdynamics Directorate. Member AIAA.

This paper is declared a work of the U.S. Government and therefore is in the public domain.

$\hat{q}_o$ = Euler solution of vortex in a uniform free stream

R = radius of rotor blade

Re = Reynolds number

r = radial distance from the vortex center

r_B = reference station on the rotor blade, fraction of R

$\vec{r}_o$ = initial vortex position, $\vec{i}x_o + \vec{j}y_o$

r_W = r/C_W

$\hat{S}$ = viscous flux vector

t = time

U,V = contravariant velocity components

$\vec{U}_\infty$ = free-stream velocity, forward velocity of rotor $\vec{i}u_\infty + \vec{j}v_\infty$

u,v = velocity components in physical plane

u_v, v_v = velocity components induced by the vortex

v_θ = tangential velocity of vortex

x_o, y_o = initial vortex location in the flow field

x_v, y_v = instantaneous vortex position

x,y,z,t = physical plane coordinates

y_b = defines airfoil surface $y_b = y_b(x,t)$

α = angle of attack

Γ = vortex strength

$\hat{\Gamma}$ = dimensionless strength of vortex $(\Gamma/U_\infty C)$

γ = ratio of specific heats

δ = airfoil thickness ratio

ε = inverse of blade aspect ratio

$\varepsilon_E, \varepsilon_I$ = explicit and implicit smoothing coefficients

θ = angle between the vortex velocity vector and y-axis

Λ = angle between vortex axis and rotor-blade chord line

μ, μ' = advance ratio and local advance ratio, respectively

$\xi_x, \xi_y, \ldots$ = metrics of transformation

ξ, η, τ = transformed plane coordinates

ρ = density

Φ = disturbance potential

Ψ = azimuth angle

Ω = angular velocity of the rotor blade

ω = reduced frequency

$(\bar{\ })$ = indicates dimensional value

Subscripts

v = vortex

∞ = free-stream condition

1. Introduction

One of the important problems of helicopter aerodynamics and one that was the subject of many recent experimental[1-4] and theoretical[5-11] studies is the mechanism of rotor blade and vortex interaction. This interaction mechanism is a primary source of impulsive noise generation. The transonic speeds of today's helicopter blade tips adds to the complexity of the problem. The blade tips, which trail the strong and concentrated tip vortices in such a flow field, trace out prolate cycloidal paths in space, and in the process encounter a variety of blade-vortex interactions. These interactions induce unsteady blade loading and aerodynamic noise, with compressibility playing an important role in the problem.

Although the generic problem of the blade-vortex interaction can be viewed in general as unsteady and three-dimensional, in one limit, when the intersection angle of the vortex with the blade is very small or zero, the interaction can be approximated to be two-dimensional but unsteady, as shown schematically in Fig. 1. Most of the recent numerical studies[5-11] that have addressed this problem have been solved in this limit. Transonic small-disturbance equations,[5-9] full-potential equations,[11] Euler equations,[7-10] and thin-layer Navier-Stokes equations[7-9] have all been solved for the problem of a convecting vortex passing and interacting with the flow field of a stationary airfoil in a uniform free stream.

Some of the above methods place limitations on the intensity of the interaction in terms of

vortex strength, of vortex location with respect to the airfoil, and on the free-stream Mach number; nevertheless, they all seem to give similar results. For flows dominated by the strong viscous interaction and shock-wave/boundary-layer interaction, the natural choice of the equation set that describes such a flow completely would be the Navier-Stokes equations. The present-day numerical algorithms for this set of equations are still very expensive in terms of computing time, although good progress has been made toward reducing the time required. But the memory of the available computers is adequate to address these kinds of problems in the two-dimensional limit. This is particularly true with the present prescribed-vortex, or perturbation, method which has been demonstrated to resolve important flow features in a blade-vortex interaction problem in both subsonic and transonic flows, even in a very sparse finite-difference mesh.[7-9]

A problem that is more practical and numerically more complicated than the one mentioned above is that of a rotating blade of a helicopter rotor encountering a vortex generated upstream. Such an experiment was done recently in a wind tunnel at the U.S. Army Aeromechanics Laboratory* at Ames Research Center.[1] A schematic of the experiment is shown in Fig. 2. A vortex generated at the tip of a straight NACA 0015 wing interacts with the flow field of a rotating, two-bladed helicopter rotor blade under subsonic and transonic flow conditions. For such a rotating blade, unlike the stationary airfoils considered in previous studies,[5-11] the unsteady time-lag effects that are present even in the absence of the interacting vortex are very important.[12] The effect of this unsteady time lag is to delay the process of adjustment of the flow corresponding to the appropriate azimuthal blade position. This has a profound influence on the unsteady blade loads. At transonic conditions this will be compounded by the presence of strong shock waves. In the results to be presented later, it will be demonstrated that these unsteady time-lag effects are important only when the flow is supercritical; they are less important if the flow is subcritical. In addition, the results may also be influenced by the three-dimensional (tip) effects, if the chordwise reference station considered is closer to the tip of the blade. Above all, one other very important ingredient of the vortex interaction study is the detailed knowledge of the structure of the interacting vortex. Although an analytical representation of the vortex is often used, the point to bear in mind is that such a representation should have an accurate core structure embedded in it.

In the present investigation, from the experimental details of Ref. 1, we find that the rotor-blade reference station (section AA in Fig. 2) that undergoes parallel blade-vortex interaction is inboard of the blade-tip region. If the tip influence is neglected at this station, the flow can be approximated as two-dimensional, but unsteady. One important difference of this problem from the earlier formulation[7-9] is that the blade is rotating now. After implementing this important feature, along with the necessary changes in the boundary conditions, unsteady, two-dimensional, thin-layer Navier-Stokes equations in strong conservation-law form are solved for the interaction flow field of the rotating blade, using an approximately factored, implicit finite-difference numerical algorithm written in delta-form.[7-9,13] An analytical representation of the measured vortex structure was used in the computations.

Although the initial finite-difference grids were generated by an algebraic method,[14] an adaptive-grid procedure[15,16] was used throughout so as to resolve the important flow features, including shock waves, vortex/shock-induced separation of the boundary layers, if any, and the vortex structure itself.

In this paper the governing equations and numerical formulations are discussed, and the numerical results and comparisons with experimental data are presented.

2. Governing Equations and Solution Procedure

The interaction flow field is solved by the *prescribed-vortex, or perturbation, method.*[17] The essence of the method is that each of the dependent flow variables is split into a prescribed part, which is simply the vortical disturbance, and a remaining part, which is obtained from the solution of the governing equation set. Even though the governing equations are nonlinear and independent solutions are not superposable, we may still decompose the dependent variables as

$$\hat{q} = \hat{q}_o + (\hat{q} - \hat{q}_o)$$

where

$$\hat{q} = \begin{bmatrix} \rho \\ \rho u \\ \rho v \\ e \end{bmatrix} \quad \text{and} \quad \hat{q}_o = \begin{bmatrix} \rho \\ \rho u \\ \rho v \\ e \end{bmatrix}_v \tag{1}$$

Here $\hat{q}$ is the unknown flow-field vector, and the vector $\hat{q}_o$ represents the solution of Euler equations for the vortical disturbance convecting in a uniform free stream. Previous studies[7-9] have demonstrated that the perturbation method can in fact resolve the flows with concentrated vortices better, even with a coarser grid, than can a non-perturbation method.[18] For example, a representative plot of the variation of lift coefficient as a function of the vortex position is reproduced from Refs. 8 in Fig. 3. This calculation was done

*Presently called Aeroflightdynamics Directorate, U.S. Army Aviation Research and Technology Activity-AVSCOM.

using Euler equations for the case of a convecting vortex encountering a nonlifting, stationary NACA 64A006 airfoil in transonic flow, and using the same grid topology with both perturbation and nonperturbation (or conventional) methods. This figure clearly demonstrates that with the conventional method the accuracy of the solution increases with the fineness of the finite-difference mesh, whereas the perturbation method produces a much better solution even in a coarser mesh.

The governing partial differential equations are the unsteady, thin-layer Navier-Stokes equations.[19] The equations are written in nondimensional, strong conservation-law form for a perfect gas using the generalized independent coordinate system of

$$\xi = \xi(x,y,t)$$

$$\eta = \eta(x,y,t) \qquad (2)$$

$$\tau = \tau(t)$$

and in the perturbation form[7-9] as

$$\partial_\tau(\hat{q} - \hat{q}_o) + \partial_\xi(\hat{E} - \hat{E}_o) + \partial_\eta(\hat{F} - \hat{F}_o) = Re^{-1}\partial_\eta\hat{S} \qquad (3)$$

where $\hat{}$ denotes quantities scaled by the Jacobian, for example

$$\hat{q} = J^{-1}q \; ; \qquad \hat{q}_o = J^{-1}q_o \qquad (4)$$

and

$$J = \xi_x\eta_y - \xi_y\eta_x = 1/(x_\xi y_\eta - x_\eta y_\xi)$$

is the transformation Jacobian. The flux vectors $\hat{E}$, $\hat{E}_o$, $\hat{F}$, $\hat{F}_o$, and $\hat{S}$ are described in detail in Refs. 7-9. The viscous flux vector $\hat{S}$ is written in the context of a thin-layer model[19] and hence is valid for high-Reynolds-number turbulent flows. The turbulent eddy viscosity is computed using a two-layer, algebraic eddy-viscosity model.[20]

The generalized coordinate system of ξ,η,τ allows the boundary surfaces in the physical plane to be mapped onto rectangular surfaces in the computational plane. This feature simplifies the procedure of grid-point clustering in the flow regions that experience rapid change in the flow-field gradients.

The primitive variables that make up the governing equations, Eq. (3), are density ρ, the two mass fluxes ρu and ρv in the two coordinate directions x and y (where x is the streamwise direction and y is normal to it), and the total energy per unit volume e. All length scales are normalized by the chord (assumed to be unity) of the rotor blade at the reference station, and the dependent variables ρ, p, e, u, and v by ρ_∞, γp_∞, $\rho_\infty a_\infty^2$, and a_∞, respectively.

The pressure, density, and velocity components are related to the energy per unit volume by the equation of state, which is written for a perfect gas as

$$e = \frac{p}{\gamma - 1} + \rho\left(\frac{u^2 + v^2}{2}\right) \qquad (5)$$

This equation of state, along with the mass and momentum equations given by Eq. (3), complete the equation set to be solved.

In the present formulation, the difference between the problems of the stationary blade and moving blade show up in the metric terms involving time derivatives, namely, ξ_t and η_t. Following the formulation given by Isom[21] and Caradonna and Isom[22] for unsteady flow over helicopter rotor blades, the effective local Mach number at the reference station can be written as

$$M_\ell = M_r(1 + \mu' \sin \omega t) \qquad (6)$$

where M_r is the rotational Mach number, μ' is the local advance ratio, and ω is the effective reduced frequency. This formulation enables the flow-field solution of a rotating blade with an oncoming free stream to be solved in the two-dimensional limit as a blade moving with an x-velocity of $M_r a_\infty \mu' \sin \omega t$ in a flow of Mach number M_r. Note that both ξ_t and η_t are nonzero for this case, whereas, for a stationary blade with a fixed grid, both ξ_t and η_t are zero.

The boundary conditions are applied explicitly. Since the grid extends 20 chord-lengths in all directions from the surface of the blade, free-stream conditions are specified at the outer boundary, and simple extrapolation is used for ρ, ρu, and ρv at the outflow boundary. For supersonic flow, the total energy e is also extrapolated, but for subsonic flow, the pressure is held constant at the free-stream value, and e is obtained from Eq. (5). To ensure continuity across the wake cut, the flow variables are linearly extrapolated to obtain the values along the cut.

Along the body surface $\eta(x,y,t) = 0$, the no-slip condition for viscous flow without suction or injection is given by setting $U = 0$ and $V = 0$. The pressure along the body surface is obtained by solving the normal momentum equation, and the density at the surface is obtained by extrapolation from the grid interior. The total energy e is calculated from the known pressure and density at the surface. The boundary conditions are of low order, and hence require that the grid be clustered and normal at the body surface. The interacting vortex is initialized, as in Ref. 9.

Surface-conforming grids are needed to simplify the application of the body-boundary condition procedure. In this study, an adaptive gridding procedure of Nakahashi and Deiwert[15,16] is used to resolve flow features and to improve the accuracy of the numerical method. Briefly, the method uses tension and torsion spring analogies. The tension spring, which connects the adjacent grid points to each other, controls grid spacings so that clustering is obtained in regions containing shock waves and shear layers. On the other hand, the torsion spring, which is attached to each grid node, controls inclinations (angles) of coordinate lines and prevents excessive grid skewness. The mesh can be made nearly orthogonal at the surface. A marching procedure is used that results in a simple tridiagonal system of equations at each coordinate line to determine the grid-point distribution. Multidirectional grid adaptation is achieved by successive application in each direction. For the compressible flow fields considered in this study, the density gradient was found to be the best choice to drive the adaption in the x-direction; the Mach number gradient was the best choice of driver in the normal direction. In actual practice, given a baseline grid, the above procedure will modify the grid at specified intervals to resolve the flow satisfactorily. In the present study, the grid was adapted at every two-marching-step intervals. This increased the computational time by about 50%. The baseline grid used was a surface-conforming C-grid generated by an algebraic method of Pulliam et al.[14] and had 221 points around the airfoil and 67 points in the normal direction. The grid boundary was chosen to be at 20 chords in all directions.

An implicit, spatially factored numerical algorithm with Euler-implicit time-differencing[13] is used to solve the perturbation-form of Eq. (3). This algorithm is written in delta form as

$$(I + h\delta_\xi \hat{A}^n - \epsilon_I J^{-1}\nabla_\xi \Delta_\xi J)(I + h\delta_\eta \hat{B}^n + h\delta_\eta \hat{M}^n$$

$$- \epsilon_I J^{-1}\nabla_\eta \Delta_\eta J)(\Delta\hat{q}^n - \Delta\hat{q}_o^n)$$

$$= -\Delta t[\delta_\xi(\hat{E}^n - \hat{E}_o^n) + \delta_\eta(\hat{F}^n - \hat{F}_o^n) - Re^{-1}\delta_\eta \hat{S}^n]$$

$$-\epsilon_E J^{-1}[(\nabla_\xi\Delta_\xi)^2 + (\nabla_\eta\Delta_\eta)^2]J(\hat{q}^n - \hat{q}_o^n) \qquad (7)$$

where $\hat{A}$, $\hat{B}$, and $\hat{M}$ are the Jacobian matrices detailed in Ref. 19; I is the identity matrix; δ_ξ, δ_η are the spatial central difference operators; and Δ and ∇ are the forward and backward difference operators. For convenience $\Delta\xi = 1 = \Delta\eta$ is assumed. The time index is denoted by h, and $\hat{q}^n = \hat{q}^n(n\Delta t)$, $\Delta\hat{q}^n = \hat{q}^{n+1} - \hat{q}^n$, and ϵ_I and ϵ_E are the implicit and explicit smoothing coefficients, respectively. Second-order implicit and fourth-order explicit numerical dissipation terms are added to the numerical scheme to improve the nonlinear stability limits posed by thefine mesh.[23] Even so, the nondimensional time-steps generally were restricted by the stability constraints to the order of 0.05° of the azimuthal travel of the blade motion or 0.005455 of the chord travel.

The numerical scheme is first-order accurate in time and second-order accurate in space. Further, in writing Eq. (7), it is assumed that $\hat{A}_o \approx \hat{A}$ and that $\hat{B}_o \approx \hat{B}$, where $\hat{A}_o = \partial\hat{E}_o/\partial\hat{q}_o$ and $\hat{B}_o = \partial\hat{F}_o/\partial\hat{q}_o$.

Central differencing is used throughout the solution domain, except in regions of supersonic flow before shock waves, where upwind differencing is used. The transformation metrics are not known analytically and are computed numerically by central differencing (second-order) at the interior points and by three-point, one-sided differencing at the boundaries.

3. Results for a Stationary Rotor Airfoil

In this section, numerical results are presented for a moving vortex encountering a fixed rotor blade under transonic conditions. All calculations are done for NACA 0012 airfoil in a uniform free stream of $M_\infty = 0.8$ at $\alpha = 0°$, and assuming a turbulent boundary layer. As mentioned earlier, an adaptive gridding procedure is used in all results presented here.

A Lamb-like vortex with a finite viscous core ($a_o = 0.05$) and a cylindrical velocity distribution given by[7-9]

$$\frac{v_\theta(r)}{a_\infty} = \frac{\hat{\Gamma}}{r} M_\infty\left(1 - e^{-r^2/a_o^2}\right) \qquad (8)$$

was chosen to interact with the flow field of a stationary, nonlifting rotor airfoil in a uniform free stream of Mach number M_∞. The strength of the vortex and its location with respect to the airfoil were chosen to be $\hat{\Gamma} = 0.2$ and $y_v = -0.26$, respectively. The interaction flow field was computed in the same manner as outlined in earlier studies.[7-9] Figure 4 shows plots of instantaneous surface-pressure distributions, the local grid arrangement, the Mach number contours, and the pressure contours for different x-locations of vortex positions as the vortex passes by the airfoil. The passing vortex induces on the airfoil a continually changing effective angle of attack. Because of the sense of rotation, it induces a downwash initially when it is upstream of the leading edge, changing to upwash as it passes behind the airfoil. This induces a continuous change in the blade-loading pattern. It should be noted here that the initial lift on the blade is zero and that any lift generated

during the interaction is induced by the vortex. As observed before,[7-9] the maximum influence of the vortex on the airfoil flow field seems to occur when the vortex is within one chord of the airfoil.

Previous calculations done for the same airfoil under identical conditions[24] used a fixed-grid topology, with 221 × 67 grid points; in that study, shocks were not well resolved. In the present case, the adaptive-grid topology, shown in Fig. 4, also uses 221 × 67 grid points, but is clearly able to resolve all aspects of the flow. Since the grid is adapted in both the x- and y-directions, it clearly resolves shock waves, the interacting vortex, and the viscous layer at the body surface. Large-scale vortex and shock-induced boundary-layer separation was not observed, although the formation of a small separation bubble and sufficient thickening of the boundary layer were seen behind shock wave for conditions when the vortex influence was maximum.

As the vortex passes the airfoil, it encounters the shock wave sitting on the surface. The vortex actually splits the shock wave into a triple shock wave, as is clearly seen from the local grid structure, Mach contours, and pressure contours of Fig. 4 for a vortex position past the midchord of the airfoil. This feature was confirmed by making a Euler calculation of the same flow, by using a fixed-grid topology, and by heavily clustering the grid in the region of interest. This apparent unsteady effect seems to fade away as the vortex passes several chords downstream of the trailing edge of the airfoil. Figure 5 shows a plot of instantaneous lift and pitching-moment coefficients as a function of the x-vortex position during the interaction process. The lift coefficient is initially negative (because of the sense of rotation of vortex), reaches a negative maximum for a vortex position slightly upstream of the leading edge of the airfoil, increases to near zero value at $x_v = 0.7$ C, and stays near that value for the rest of the interaction period. Pitching-moment changes are maximum when the vortex is within 1 C of the airfoil.

4. Results for a Rotating Blade

In this section, computational results are presented corresponding to two experimental conditions of Caradonna et al.[1] One condition each of subcritical and supercritical flows with and without vortex encounter will be discussed. The corresponding tip Mach number of the two cases is 0.6 and 0.8, respectively, with an advance ratio $\mu = 0.2$ for both.

The schematic of the experimental arrangement is shown in Fig. 2. The experiments were performed in a wind tunnel where a NACA 0015 wing generated a tip vortex upstream of a two-bladed, model helicopter rotor. The interacting vortex, of core radius 25 mm, passed the reference rotor spanwise station at $r_B = 0.893$ and at a distance of $y_v = -0.4$ C. The chord of the rotor blade was 152.4 mm, and the diameter of the rotor was 2.134 m.

Structure of the Experimental Vortex

Comparisons of numerical results and the above experimental data will be meaningful only if we consider the correct structure of the experimental vortex. The information about the vortex core size and the strength alone is not sufficient to describe the correct vortex structure. Since the vortex peak velocity determines to a large extent the induced effects caused by the vortex interaction, an analytical representation of the cylindrical velocity field, such as that of Eq. (8), based just on the vortex strength $\hat{\Gamma}$ and the core radius a_o may, in fact, give a totally different vortex structure. Comparison of the cylindrical velocity distribution of the measured data of Takahashi and McAlister[25] and of Orloff and Grant[26] with that calculated from Eq. (8) using $a_o = 25$ mm and $\hat{\Gamma} = 0.31$ reported by Caradonna et al.[1] showed a 40% greater peak velocity and a different distribution, although it had the inviscid vortex, 1/r, behavior well outside the viscous core.

To circumvent this problem, we have put together all the available NACA 0015 data[25,26] that were obtained under similar conditions into one plot (Fig. 6) of cylindrical velocity distribution as a function of the distance from the vortex center. Based on some of the arguments presented by Iversen[27] in correlating a large mass of data (particularly $v_{\theta_{max}}$ on turbulent trailing vortex decay, the experimental data of Fig. 6 could be represented by an analytical expression, similar to Scully's viscous vortex,[28] by

$$\frac{v_\theta}{U_\infty} = \frac{0.8\hat{\Gamma}}{2\pi r_w}\left(\frac{r_w^2}{r_w^2 + a_{ow}^2}\right) \qquad (9)$$

The core radius a_o was taken to be 25 mm, as reported by Caradonna et al.[1] and in agreement with Refs. 25-26. With this a_o, the value of $\hat{\Gamma}$ was chosen to match the data of Orloff and Grant[26] for $v_{\theta_{max}}$. This analytical fit to the experimental data is also shown in Fig. 6 along with 1/r behavior of an inviscid vortex. Based on this analytical description, the strength of the vortex was found to be only 80% of the value quoted by Caradonna et al.[1]

Subcritical Case

This condition corresponds to $M_T = 0.6$ and $\mu = 0.2$. For the reference station at 89.3% of the rotor blade radius, these conditions translate to $M_r = 0.536$ and $\mu' = 0.223$.

Results for Rotor Alone. First we consider a nonlifting rotor in forward flight in the absence of vortex interaction. The objective of such an exercise is to determine the importance of three-dimensional, unsteady time-lag effects as the rotor sweeps in azimuth, say from 0°-180°. As the blade rotates from 0°-180°, its effective Mach number increases in the first quadrant, reaching a maximum at the $\psi = 90 + \Delta\psi$ position; it again decreases to the average value at $\psi = 180°$. In going through this change in local Mach number, if the flow on the rotor at $\psi = 180°$ is nearly the same as that at $\psi = 90 - \Delta\psi$, the the rotating blade behaves as if it were quasi-steady and quasi-two-dimensional. If, on the other hand, the two flows are different, then the associated three-dimensional time-lag effects will have an influence on the vortex-blade interaction flow field that develops in the vicinity of the $\psi = 180°$ position.

Figure 7 shows a sequence of instantaneous surface-pressure results at several azimuthal positions of the blade. For this flow, the initial local Mach number for $\psi = 0°$ is 0.536 and increases to a maximum (based on the local advance ratio) at $\psi = 90°$ and again decreases to 0.536 at $\psi = 180°$. Examination of these pressure distributions indicates that for this subcritical flow condition, the unsteady time-lag effects are negligible.

Vortex Encounter with a Rotating Blade. To compute the vortex interaction flow field, as before, the vortex was initialized at the $\psi = 0°$ position of the rotor blade (the corresponding $x_v = -19.638$) as in Refs. 7-9. It then convects with the flow at the effective "free-stream velocity," which is $M_r a_\infty(1 + \mu' \sin\psi)$ in this case. Typical instantaneous surface-pressure distributions are shown in Fig. 8 corresponding to several vortex positions as the vortex convects past the rotor blade. Since the rotor is a nonlifting one, the lift is initially zero, and, as the vortex approaches the blade, it induces a downwash and hence a negative lift. This continuously increases and reverses in sign, becoming positive lift as the vortex passes the airfoil. Shown in this figure are data from the experiments of Caradonna et al.[1] The comparison of numerical results and experimental data show good agreement, both qualitatively and quantitatively; the peak pressures on the nonvortex side of the blade seem to be underpredicted. It should be pointed out here that in the experiments, the rotor model had pressure taps on only one surface. To get the pressure distribution on both the surfaces, the model was simply inverted and a second, almost identical, experiment was run. Nevertheless, it is gratifying to see such a good agreement with experiments. So far we have neglected the three-dimensional effects, if any exist. Even if three-dimensional effects are present, because of the proximity of the reference station to the blade tip region, their influence at this flow condition appears minimal.

Supercritical Case

This condition corresponds to a tip Mach number of 0.8, with an advance ratio of 0.2, and the blade reference station $r_B = 0.893$, as before. This translates to a reference Mach number of 0.714 and a local advance ratio μ' of 0.223.

Results for Rotor Alone. We first present results for the rotor-alone case (i.e., in the absence of vortex interaction). Figure 9 shows plots of instantaneous surface-pressure distributions at four rotor-blade azimuthal positions. For this case, the initial lift on the rotor blade (at $\psi = 0°$) is zero, and the flow is subcritical; but as the blade rotates, its local effective Mach number increases, reaching a maximum at $\psi = 90°$ and decreasing in the second quadrant. As seen in these pressure-distribution plots, the shock wave that develops as the blade rotates gets stronger and moves toward the trailing edge of the airfoil. Even though the effective local Mach number reaches a maximum for $\psi = 90°$, the shock wave continues to get stronger and move toward the trailing edge in the second quadrant before it starts moving upstream toward the leading edge of the blade. This unsteady time lag in the growth and decay of the shock wave persists, even when the rotor blade has passed the 180° azimuthal position into the third quadrant.

Comparison of experimental data[29] with numerical results in Fig. 9 shows relatively good agreement as far as the pressure levels are concerned for all azimuthal positions of the blade up to $\psi = 150°$, but the location of the shock wave is too far aft in the second quadrant. In the experiments, the shock wave seems to have collapsed between $\psi = 150°$ and $\psi = 180°$. But the numerical results show the survival of a strong shock wave even at $\psi = 180°$, as discussed below. This suggests the presence of possible three-dimensional effects besides the unsteady shock-wave lag effects.

Some insights into possible three-dimensional influences can be obtained from the transonic small-disturbance equation for a thin, high-aspect-ratio rotating blade[21]:

$$A\phi_{tt} + B\phi_{xt} = \frac{\partial}{\partial x}\left[C_1\phi_x + C_2\phi_x^2\right] + \phi_{yy} + D\phi_{xz} + E\phi_{zz} \qquad (10)$$

As discussed in the Appendix, this equation reveals by inspection that three-dimensional effects influence the solution through the two terms $D\phi_{xz}$ and $E\phi_{zz}$, where

$$D = -2M_r\epsilon\mu' \cos t(z + \mu' \sin t)/\delta^{2/3}$$

and

$$E = \epsilon^2/\delta^{2/3}$$

Of these two terms, the coefficient E in the latter is independent of Mach number, and $E\phi_{zz}$ is undoubtedly important in the immediate vicinity of the tip of the rotor blade. On the other hand, the former term $D\phi_{xz}$, is clearly dependent on Mach number, and the coefficient D is also a strong function of the blade aspect ratio, the azimuth of the rotor blade, the spanwise station along the blade, and the local advance ratio, $\mu' = U_\infty/\Omega r_B$, of the rotor. Therefore, it seems likely that this term might play the dominant three-dimensional role inboard of the tip, especially under transonic conditions.

A qualitative estimate of the influence of this cross-flow term has been deduced from two-dimensional calculations in which $D\phi_{xz}$ was added ad hoc as an inhomogeneous "source" term to the basic small-disturbance code ATRAN2 (Ref. 30), as discussed in the Appendix. Namely, $\phi_{xz}(x,y,z,t) = F'(z)\phi_x(x,y,t)$ was evaluated by assigning an arbitrary constant to F'/F at a fixed $z = r_B$, and by evaluating ϕ_x at the previous time-step. It was found that negative values of F'/F tended to strengthen the shock wave for $0 < \psi < 90$ and to weaken it for $90 < \psi < 180$; positive values of F'/F had the opposite effect. The sensitivity of the calculated results to the value of F'/F is illustrated in Fig. 10, at $\psi = 150°$ and $180°$ for the example considered in Fig. 9. Figure 10 shows, especially at the 180° azimuthal position, a drastic alteration of the shock-wave strength and position with increases in the magnitude of the cross-flow term.

Figure 11 shows a comparison of the experimental pressure distributions, the Navier-Stokes calculations, and the transonic small-disturbance calculations with and without the above three-dimensional correction. The two-dimensional ATRAN2 and thin-layer Navier-Stokes results are in good agreement, and both calculations show the persistence of the strong shock wave for $\psi = 180°$. On the other hand, the three-dimensional correction modifies the ATRAN2 results into closer agreement with the experimental data, and the calculated shock wave at $\psi = 180°$ has almost vanished.

It must be emphasized that the above analysis is only intended to demonstrate the potential importance of cross-flow effects in supercritical flow, and not to predict accurately such an effect. Although it seems logical that three-dimensional effects should depend on M_r, μ', ψ, and ϵ in the manner suggested by the coefficient E in Eq. (10), the separation of variables $\phi(x,y,z,t) = F(z)\phi(x,y,t)$ is only an assumption, and the choice of F'/F is purely arbitrary. Nevertheless, the results in Figs. 9-11 clearly demonstrate that the rotor-alone supercritical case under consideration is neither quasi-two-dimensional nor quasi-steady. This stands in sharp contrast with the previous subcritical case, Figs. 7 and 8, for which the two-dimensional numerical calculations are in excellent agreement with the model rotor data, and for which the significant unsteady effects are only a result of the airfoil-vortex interaction.

Vortex Interaction with a Rotor Blade Section. A previous attempt[9] to compute the blade-vortex interaction flow field, for the supercritical flow case without considering the unsteady time-lag effects produced unsatisfactory results in terms of agreement with experiments. Typical results, reproduced from Ref. 9, are shown in Fig. 12. First indications of poor agreement with experiments are the absences of strong shock waves which is a consequence of neglecting unsteady lag effects of the rotating blade. The results presented in Figs. 9-11 show not only the importance of unsteady time-lag effects, but also the three-dimensional influence for this flow.

Based on the arguments presented above, the blade-vortex interaction flow field at this supercritical condition is calculated, using the two-dimensional, transonic small-disturbance equations with the three-dimensional correction. As shown in Fig. 10, the calculations are sensitive to the value of the three-dimensional correction factor B1. From the results presented in Figs. 9-11, a value of $B1 = 0.2$ gave the best match with experimental data[29] for the rotor azimuthal position of 180°. This value for B1 was used in the blade-vortex interaction calculations.

Figure 13 shows the results of these calculations compared with the experimental data.[1] The results are in good qualitative agreement. Although the calculations show good quantitative agreement with the experiments at the $xv = -0.35$ station, the agreement seems to degrade progressively as the vortex passes downstream of the blade. It should be noted that the flow on the blade is subcritical (with zero lift) in the absence of the vortex interaction for $\psi = 180°$ (see Fig. 11). With the vortex interaction, the flow on the blade becomes supercritical, with strong shock waves as the interaction effects peak. As the vortex passes downstream of the blade, these supercritical conditions progressively change to subcritical conditions. Also, because of the vortex interaction, the blade develops lift which is initially negative (because of the sense of rotation of the vortex), becoming positive as the vortex passes the blade.

In view of the strong viscous interaction inherent in this present problem, it is not surprising to see less-than-perfect agreement between calculations and experimental data. Probably this is a limitation of this present method. Nevertheless, it has demonstrated the importance of the three-dimensional effects in the presence of shock waves. An additional important observation indicates that if the calculated results are lagged by about 2.5° of azimuthal position (or about a quarter chord of travel), the calculations seem to show better quantitative agreement with

experiments for all x-positions of the vortex. Typical pressure distributions, replotted with this phase shift of a quarter chord, are shown in Fig. 14.

5. Concluding Remarks

This paper presents a computational procedure for calculating the interaction flow field of a passing vortex with a helicopter rotor blade in forward flight, as well as numerical results for subsonic and transonic flow conditions. The interaction of the vortex considered here is one of the limiting cases of a more complex interaction typically encountered on a helicopter rotor blade, and it corresponds to the parallel blade-vortex interaction experimental conditions of Caradonna et al.[1] In this limit, the interaction flow field can be approximated to be two-dimensional and unsteady. The numerical scheme involves the solution of unsteady, two-dimensional, thin-layer Navier-Stokes equations implicitly using the prescribed-vortex, or perturbation, approach presented in Refs. 7-9.

The computational procedure is very general and accepts any arbitrary size and shape of the interacting vortex, although the structure of the vortex is assumed to remain unaltered by the interaction. For comparing the present numerical results with the experiments, it was found that the details of the vortex structure were important. Accordingly, experimental data on the vortex cylindrical velocity distribution were used to describe the vortex analytically, and this was used in the computations.

Two test cases, subsonic and transonic conditions corresponding to the experimental data, were chosen for the calculations. The respective blade-tip Mach numbers were 0.6 and 0.8, and the blade advance ratio was 0.2. A comparison of the numerical results for these two conditions showed a very distinct difference in the flow fields, even in the absence of the interacting vortex.

The results show that for the subcritical case, the unsteady time-lag effects are negligible for the rotating blade in the absence of the vortex and that the unsteady flow field with the vortex interaction is in very good qualitative and quantitative agreement with experiments. The supercritical case, however, is totally dominated by strong (transonic) shock waves, the consequence of which is the presence of strong, unsteady time-lag effects, even in the absence of the vortex interaction. In addition, there are strong indications of the influence of three-dimensional effects. The experimental data for the rotor-alone case show the collapse of the shock wave between blade azimuthal positions of 150° and 180°. The numerical results, on the other hand, show the persistence of a strong shock wave even at 180°.

The influence of three-dimensional effect was further examined by using a modification of the ATRAN2 code (two-dimensional, transonic, small-disturbance code). An ad hoc three-dimensional correction was added to the ATRAN2 code to introduce the cross-flow effect along the blade. Calculations done with this modified ATRAN2 code for the rotor-alone case showed the collapse of the strong shock wave between the azimuthal positions of 150° and 180°, and the calculations showed good qualitative and fairly good quantitative agreement with experiments. The vortex interaction flow field for this supercritical condition was calculated using this modified ATRAN2 code. The results show good agreement with experiments when the vortex is near the leading edge of the blade, but seem to degrade progressively as the vortex passes the airfoil. In view of the strong viscous interaction inherent in this problem, it is not surprising to see less-than-perfect agreement between these results and those of experiments. Probably this is a limitation of this approximate method. Nevertheless, it has demonstrated the importance of the three-dimensional effects at these supercritical conditions.

A similar calculation done with this approximate method for the subcritical case showed almost no three-dimensional influence, suggesting that three-dimensional effects, if any, seem to be accentuated in the presence of shock waves.

Appendix

The three-dimensional, transonic small-disturbance equation for a thin, high-aspect-ratio rotating blade, as derived by Isom,[21] is

$$A\phi_{tt} + B\phi_{xt} - \frac{\partial}{\partial x}\left[C_1\phi_x + C_2\phi_x^2\right] - \phi_{yy} - D\phi_{xz} - E\phi_{zz} \qquad (A1)$$

where

$$A = M_r^2\epsilon^2/\delta^{2/3}$$

$$B = 2M_r^2\epsilon(z + \mu' \sin t)/\delta^{2/3}$$

$$C_1 = [1 - M_r^2(z + \mu' \sin t)]/\delta^{2/3}$$

$$C_2 = 1/2(\gamma + 1)M_r^2(z + \mu' \sin t)$$

$$D = -2M_r^2\epsilon\mu' \cos t(z + \mu' \sin t)/\delta^{2/3}$$

$$E = \epsilon^2/\delta^{2/3}$$

$$\phi = \bar{\phi}/(\Omega\bar{R}_r\bar{c}\delta^{2/3})$$

$$\epsilon = \bar{c}/\bar{R}_r$$

$$\mu' = v_\infty/\Omega\bar{R}_r$$

$$M_r = \Omega\bar{R}_r/a_\infty$$

$$x = \bar{x}/\bar{c}$$

$$y = \bar{y}/\bar{c}$$

$$z = \bar{z}/\bar{R}_r$$

$$t = \Omega\bar{R}_r\bar{t}/\bar{R}_r = \Omega\bar{t}$$

$$\bar{R}_r = \bar{r}_B$$

In this equation, Φ is the disturbance potential, z is the spanwise coordinate, and x,y remain the blade airfoil coordinates as defined in Section 2 of the text. The variables are scaled by the airfoil thickness ratio μ, and by the inverse of the blade aspect ratio ϵ, following the standard, small-disturbance scaling arguments for transonic flows[21]; namely,

$$1 - M_r^2(z + \mu') = O(\epsilon) = O(\delta^{2/3}) \qquad (A2)$$

For the purposes of this investigation, the reference conditions in Eq. (A1) are defined for the experimental rotor of Caradonna et al.[1] as follows: $\bar{c}$ is the chord of the rotor blade; $\bar{r}_B$ is the radius of the spanwise station where the measurements were reported, that is, at $r_B = 89.3\%$ of the blade radius; $M_r = \Omega r_B/a_\infty^2$ is the rotational Mach number at the measurement station; and U_∞ is the free-stream velocity of the wind tunnel.

Spanwise gradients that could introduce strong three-dimensional effects appear only in the two terms, $D\Phi_{xz}$ and $E\Phi_{zz}$, in Eq. (A1). An approximate, qualitative indication of how these terms might alter the two-dimensional "strip-theory" characteristics of the flow past a rotor blade can be obtained by considering a separation of variables:

$$\Phi(x,y,z,t) = \tilde{\Phi}(x,y,t)F(z) \qquad (A3)$$

Then Eq. (A1) becomes

$$A\tilde{\Phi}_{tt} + B\tilde{\Phi}_{xt} - (C_1\tilde{\Phi}_x + C_2\tilde{\Phi}_x^2)_x - \tilde{\Phi}_{yy} - D\tilde{\Phi}_x F'/F - E\tilde{\Phi}F''(z)/F(z) \qquad (A4)$$

where the prime denotes differentiation with respect to z.

As a further approximation, we exclude the tip region, thereby neglecting the term $E\tilde{\Phi}F''/F$, and assume that the three-dimensional effects are only small perturbations on the basic two-dimensional solution at the spanwise station in question, $z = z/r_B = 1$. This allows us to treat $D\tilde{\Phi}_x F'/F$ as an inhomogeneous "source" term, which we shall evaluate numerically at the previous time-step, once a suitable approximation to $F'(z)/F(z)$ has been determined.

Within this framework, our previous prescribed-disturbance formulation[8,30] for vortical flows and the basic numerical algorithm for solving the governing equation can be implemented with only minor changes. That is, we write

$$v\tilde{\Phi} = v\Phi + \vec{q}_v \qquad (A5)$$

where $\vec{q}_v$ is the prescribed velocity field induced by the vortex in the absence of the rotor blade, as explained in the text. Then the governing equation for Φ is

$$A\Phi_{tt} + B\Phi_{xt} - [C_1\Phi_x + C_2\Phi_x(\Phi_x + u_v)]_x - \Phi_{yy} = D\Phi_x^n F'(z)/F(z) \qquad (A6)$$

The left-hand side of Eq. (A6) is unchanged from Refs. 7 and 30, except that the coefficients B, C_1, and C_2 now contain the factor $(1 + \mu' \sin t)$, which was not included before (see also Ref. 12). The value of Φ_x is known from the solution of Eq. (A6) at the previous time-step; the function $F(z)$ has to be specified.

The boundary condition on the blade profile is

$$\Phi_y(y = 0) = (1 + \mu' \sin t)\frac{\partial y_b}{\partial x} + \epsilon\frac{\partial y_b}{\partial t} \pm \frac{\alpha}{\delta} - v_v \qquad (A7)$$

and the wake condition of zero pressure jump across the airfoil branch cut is

$$[(1 + \mu' \sin t)\Gamma_x + \epsilon\Gamma_t]_{wake} = 0 \qquad (A8)$$

The pressure coefficient is given by

$$C_p = -\frac{2\Phi_x}{1 + \mu' \sin t} - \frac{2\epsilon\Phi_t}{(1 + \mu' \sin t)^2} \qquad (A9)$$

Equations (A6)-(A9) have been solved using the basic code ATRAN2 (Ref. 30) with minor modifications, for specified values of the quantity $F'(z = 1)/F(z = 1)$.

Acknowledgments

The research of the first author (GRS) is supported by the U.S. Army Research Office Contract DAAG29-85-C-0002. We would like to express our sincere thanks to Dr. J. L. Steger for some stimulating discussions.

References

[1]Caradonna, F. X., Laub, G. H., and Tung, C., "An Experimental Investigation of the Parallel Blade-Vortex Interaction," Paper No. 4, Tenth European Rotorcraft Forum, The Hague, Netherlands, Aug. 1984.

[2]McAlister, K. W. and Tung, C., "Airfoil Interaction with an Impinging Vortex," NASA TP-2273, 1984.

[3]Meier, G. E. A. and Timm, R., "Unsteady Vortex Airfoil Interaction," Paper No. 16, AGARD CP-386, AGARD Symposium on Unsteady Aerodynamics: Fundamentals and Applications to Aircraft Dynamics, May 1985.

[4]Padakannaya, R., "Experimental Study of Rotor Unsteady Airloads due to Blade-Vortex Interaction," NASA CR-1907, 1971.

[5]Caradonna, F. X., Tung, C., and Desopper, A., "Finite-Difference Modeling of Rotor Flows Including Wake Effects," Journal of the American Helicopter Society, Vol. 29, No. 2, Apr. 1984, pp. 26-33.

[6]George, A. R. and Chang, S. B., "Noise due to Transonic Blade-Vortex Interactions," Paper A-83-39-50-D000, 39th Annual National Forum of the American Helicopter Society, May 1983.

[7]Srinivasan, G. R., McCroskey, W. J., and Kutler, P., "Numerical Simulation of the Interaction of a Vortex with a Stationary Airfoil in Transonic Flow," AIAA Paper 84-0254, Reno, Nev., 1984.

[8]McCroskey, W. J. and Srinivasan, G. R., "Transonic Interaction of Unsteady Vortical Flows," Paper No. 5-1, Third Symposium of Numerical and Physical Aspects of Aerodynamic Flows, Long Beach, Calif., Jan. 1985. (Also NASA TM-86658, 1984.)

[9]Srinivasan, G. R., "Computations of Two-Dimensional Airfoil-Vortex Interactions," NASA CR-3885, 1985.

[10]Wu, J. C., Sankar, N. L., and Hsu, T. M., "Unsteady Aerodynamics of an Airfoil Encountering a Passing Vortex," AIAA Paper 85-0203, Reno, Nev., 1985.

[11]Jones, H. E., "The Aerodynamic Interaction between an Airfoil and a Vortex in Transonic Flow," Paper presented at the Workshop on Blade-Vortex Interactions (unpublished), Moffett Field, Calif., Oct. 1984.

[12]Caradonna, F. X. and Philippe, J.-J., "The Flow over a Helicopter Blade Tip in the Transonic Regime," Vertica, Vol. 2, No. 1, 1978, pp. 43-60.

[13]Beam, R. M. and Warming, R. F., "An Implicit Finite-Difference Algorithm for Hyperbolic Systems in Conservation-Law Form," Journal of Computational Physics, Vol. 22, Sept. 1976, pp. 87-109.

[14]Pulliam, T. H., Jespersen, D. C., and Childs, R. E., "An Enhanced Version of an Implicit Code for the Euler Equations," AIAA Paper 83-0344, Reno, Nev., 1983.

[15]Nakahashi, K. and Deiwert, G. S., "A Practical Adaptive-Grid Method for Complex Fluid-Flow Problems," Lecture Notes in Physics, Vol. 218, Springer-Verlag, 1984, pp. 422-426. (Also NASA TM-85989, 1984.)

[16]Nakahashi, K. and Deiwert, G. S., "A Self-Adaptive-Grid Method with Application to Airfoil Flow," AIAA Paper 85-1525-CP, Cincinnati, Ohio, 1985.

[17]Buning, P. G. and Steger, J. L., "Solution of the Two-Dimensional Euler Equations with Generalized Coordinate Transformation Using Flux Vector Splitting," AIAA Paper 82-0971, St. Louis, Mo., 1982.

[18]Srinivasan, G. R., Chyu, W. J., and Steger, J. L., "Computation of Simple Three-Dimensional Wing Vortex Interaction in Transonic Flow," AIAA Paper 81-1206, Palo Alto, Calif., 1981.

[19]Steger, J. L., "Implicit Finite-Difference Simulation of Flow about Arbitrary Two-Dimensional Geometries," AIAA Journal, Vol. 16, No. 7, July 1978, pp. 679-686.

[20]Baldwin, B. S. and Lomax, H., "Thin Layer Approximation and Algebraic Model for Separated Turbulent Flows," AIAA Paper 78-257, Huntsville, Ala., 1978.

[21]Isom, M. P., "Unsteady Subsonic and Transonic Potential Flow over Helicopter Rotor Blades," NASA CR-2463, 1974.

[22]Caradonna, F. X. and Isom, M. P., "Numerical Calculation of Unsteady Transonic Potential Flow over Helicopter Rotor Blades," AIAA Journal, Vol. 14, No. 4, Apr. 1976, pp. 482-488.

[23]Pulliam, T. H. and Steger, J. L., "On Implicit Finite-Difference Simulations of Three-Dimensional Flow," AIAA Journal, Vol. 18, No. 2, Feb. 1980, pp. 159-167.

[24]Srinivasan, G. R. and McCroskey, W. J., "Computations of Blade-Vortex Interaction by Different Methods," Paper presented at the Workshop on Blade-Vortex Interactions (unpublished), Moffett Field, Calif., Oct. 1984.

[25]Takahashi, R. K. and McAlister, K. W., "Preliminary Measurements of a Wing-Tip Vortex using Laser Velocimetry," private communication, 1985.

[26]Orloff, K. L. and Grant, G. R., "The Application of Laser Doppler Velocimetry to Trailing Vortex Definition and Alleviation," NASA TM X-62,243, 1973.

[27]Iversen, J. D., "Correlation of Turbulent Trailing Vortex Decay Data," Journal of Aircraft, Vol. 13, No. 5, May 1975, pp. 338-342.

[28]Scully, M. P., "Computation of Helicopter Rotor Wake Geometry and Its Influence on Rotor Harmonic Loads," ASRL TR-178-1, Massachusetts Institute of Technology, Mar. 1975.

[29]Tung, C., private communication, 1985.

[30]McCroskey, W. J. and Goorjian, P. M., "Interactions of Airfoils with Gusts and Concentrated Vortices in Unsteady Transonic Flow," AIAA Paper 83-1691, Danvers, Mass., 1983.

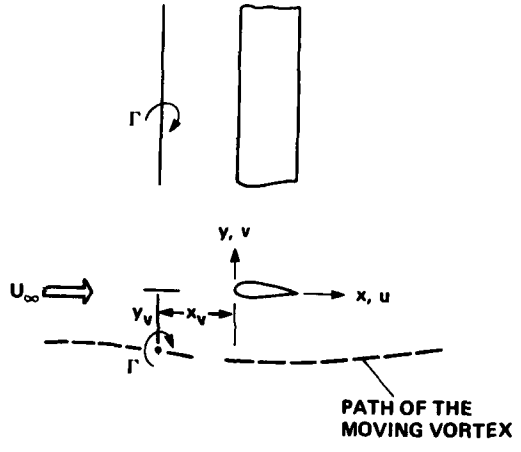

Fig. 1 Schematic of parallel blade-vortex interaction, in the limit of $M = 0$, and definition of coordinate system.

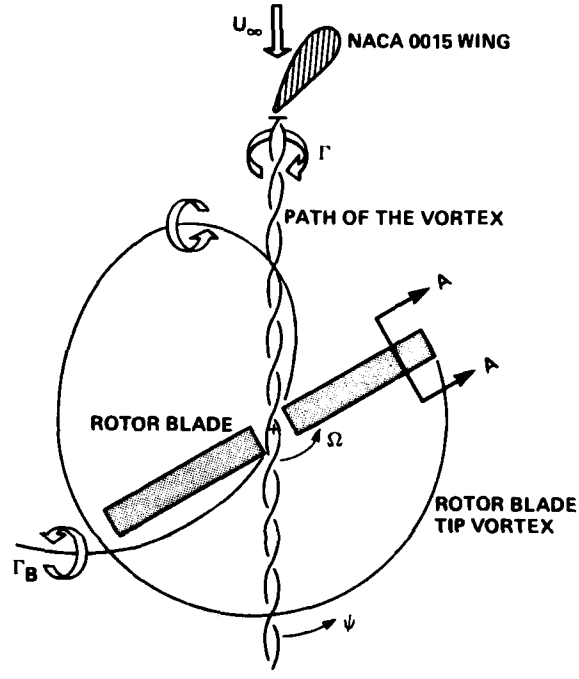

Fig. 2 Schematic of experimental model rotor tests.

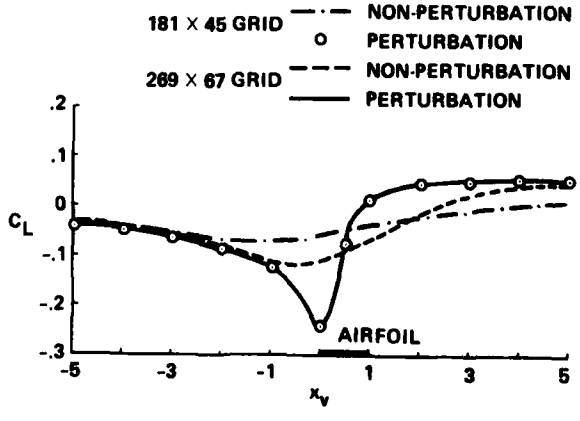

Fig. 3 Effectiveness of the prescribed-vortex method compared with the nonperturbation method. Euler results for airfoil-vortex interaction: NACA 64A006 airfoil, $M_\infty = 0.85$, $\alpha = 0°$, $\hat{\Gamma} = 0.2$, $a_o = 0.05$, and $y_o = y_v = -0.26$.

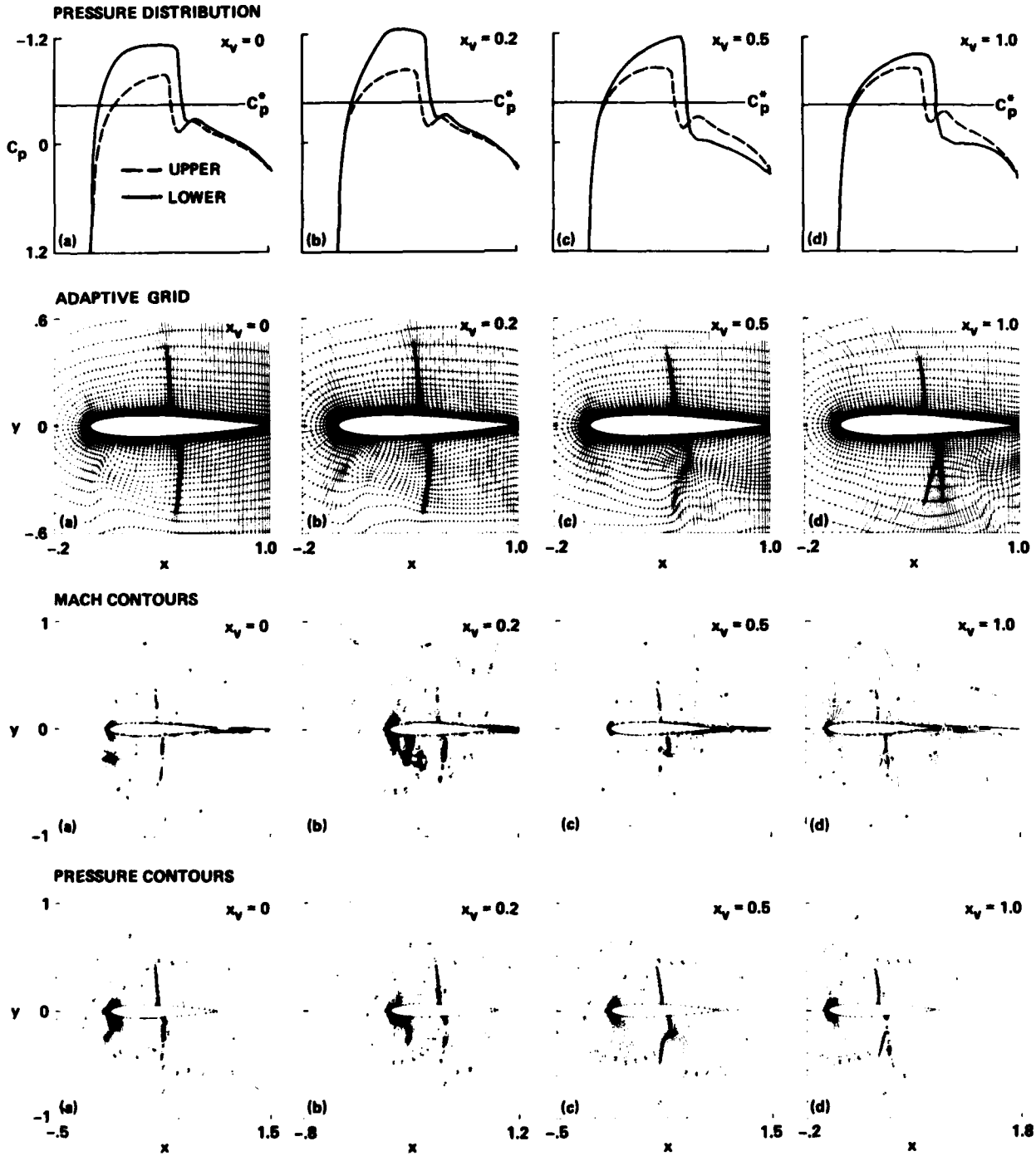

Fig. 4 Instantaneous surface-pressure distributions, adaptive grid, Mach contours, and pressure contours during airfoil-vortex interaction with a convecting vortex: NACA 0012 airfoil, $M_\infty = 0.8$, $\alpha = 0°$, Re = 2×10^6 per meter, $\hat{\Gamma} = 0.2$, $y_o = y_v = -0.26$.

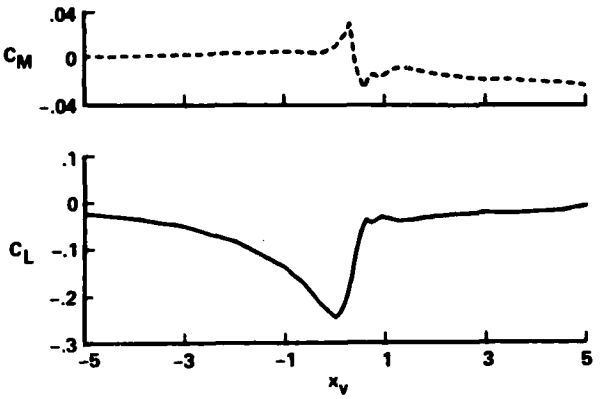

Fig. 5 Lift and pitching-moment variations with instantaneous vortex position for the conditions of Fig. 4.

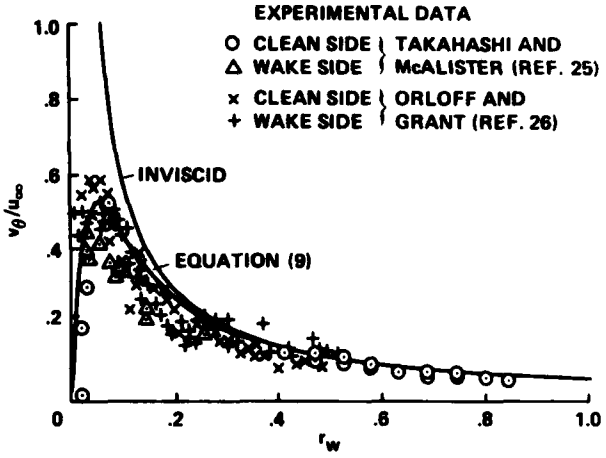

Fig. 6 Tangential velocity distribution of the tip vortex generated by NACA 0015 wing.

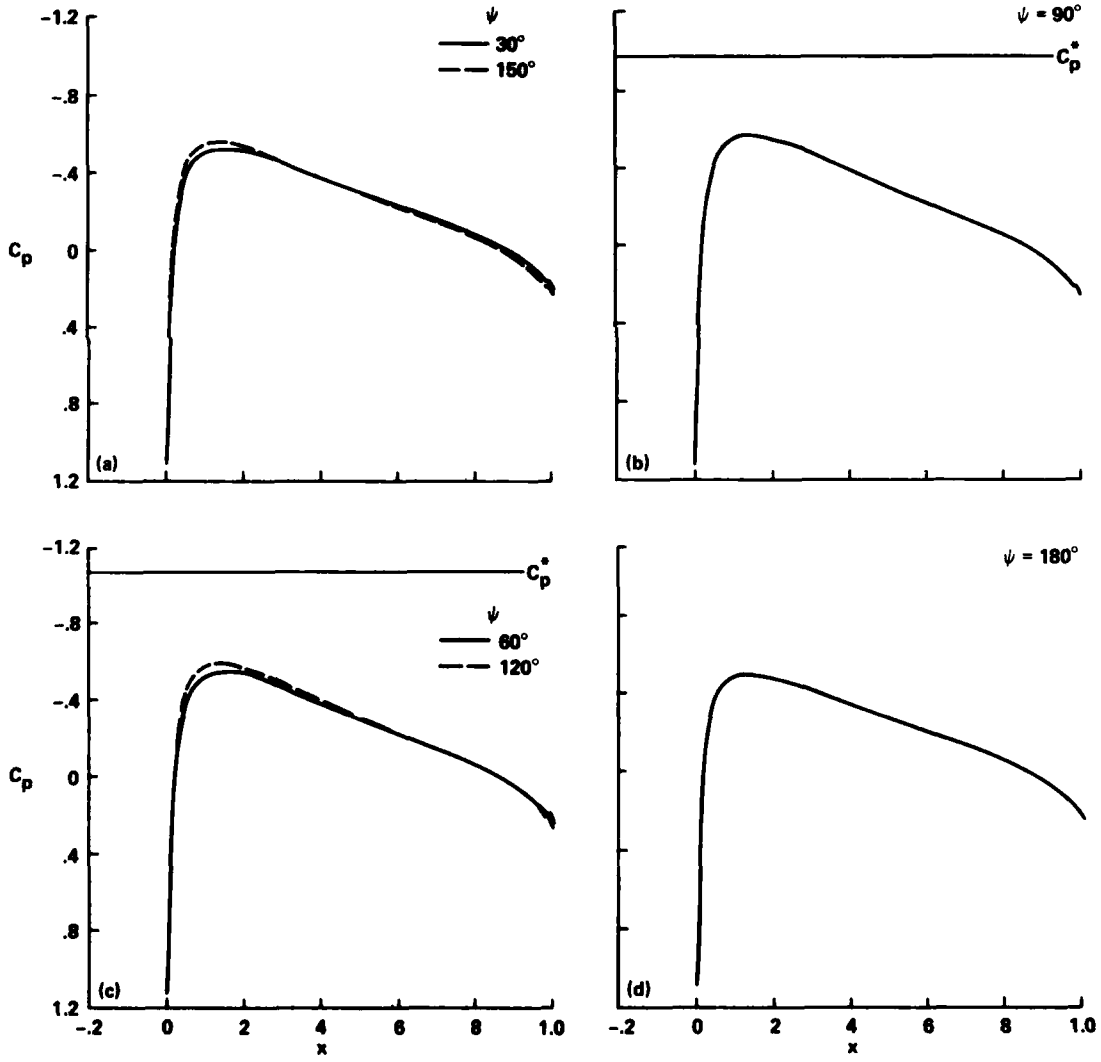

Fig. 7 Instantaneous pressure distributions at the reference blade station for the rotor-alone case: $M_T = 0.6$, $\mu = 0.2$, $r_B = 0.893$.

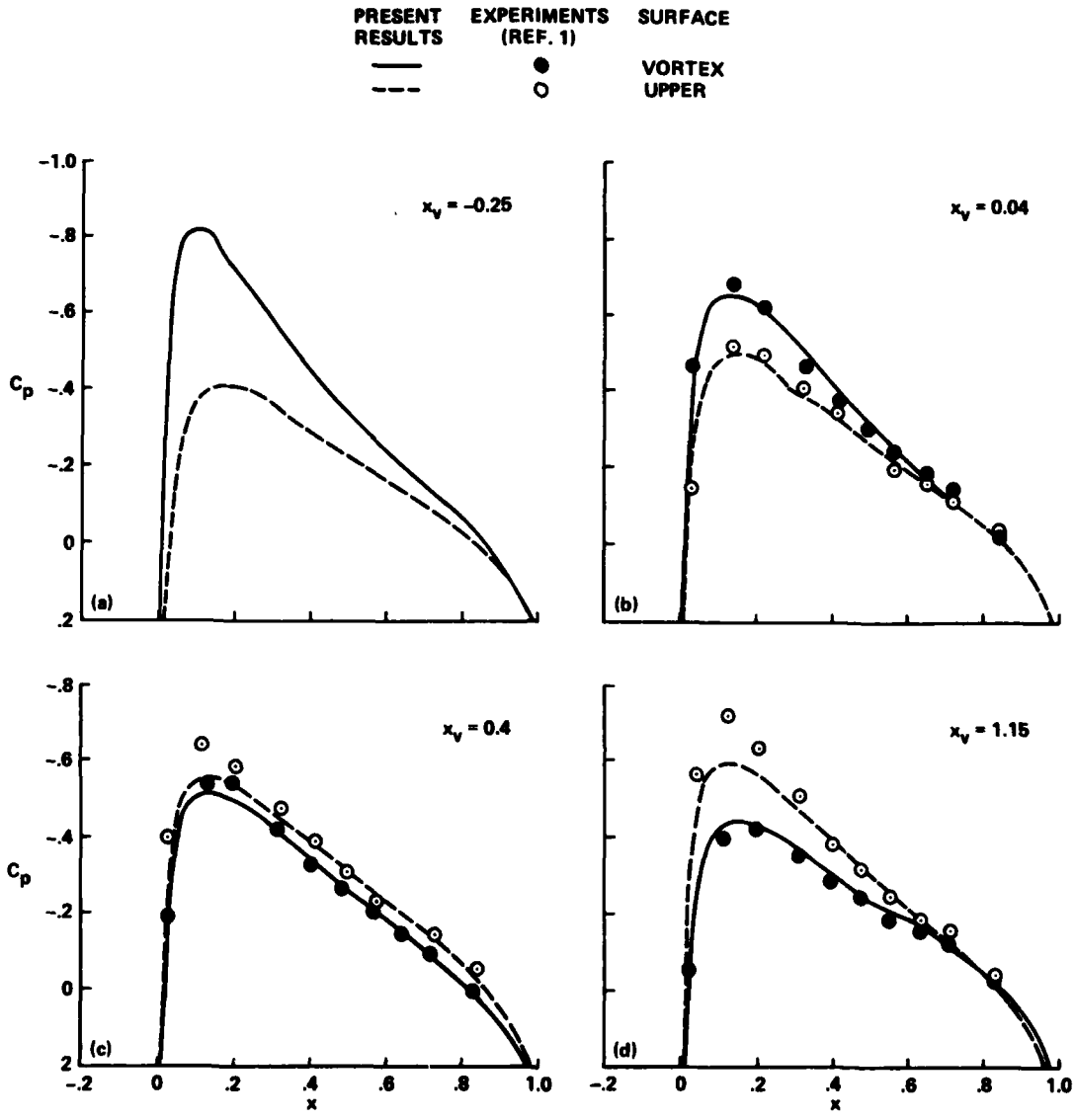

Fig. 8 Instantaneous surface-pressure distributions for the case of blade-vortex interaction: $M_T = 0.6$, $\mu = 0.2$, $r_B = 0.893$, $\hat{\Gamma} = 0.243$, $y_v = -0.4$.

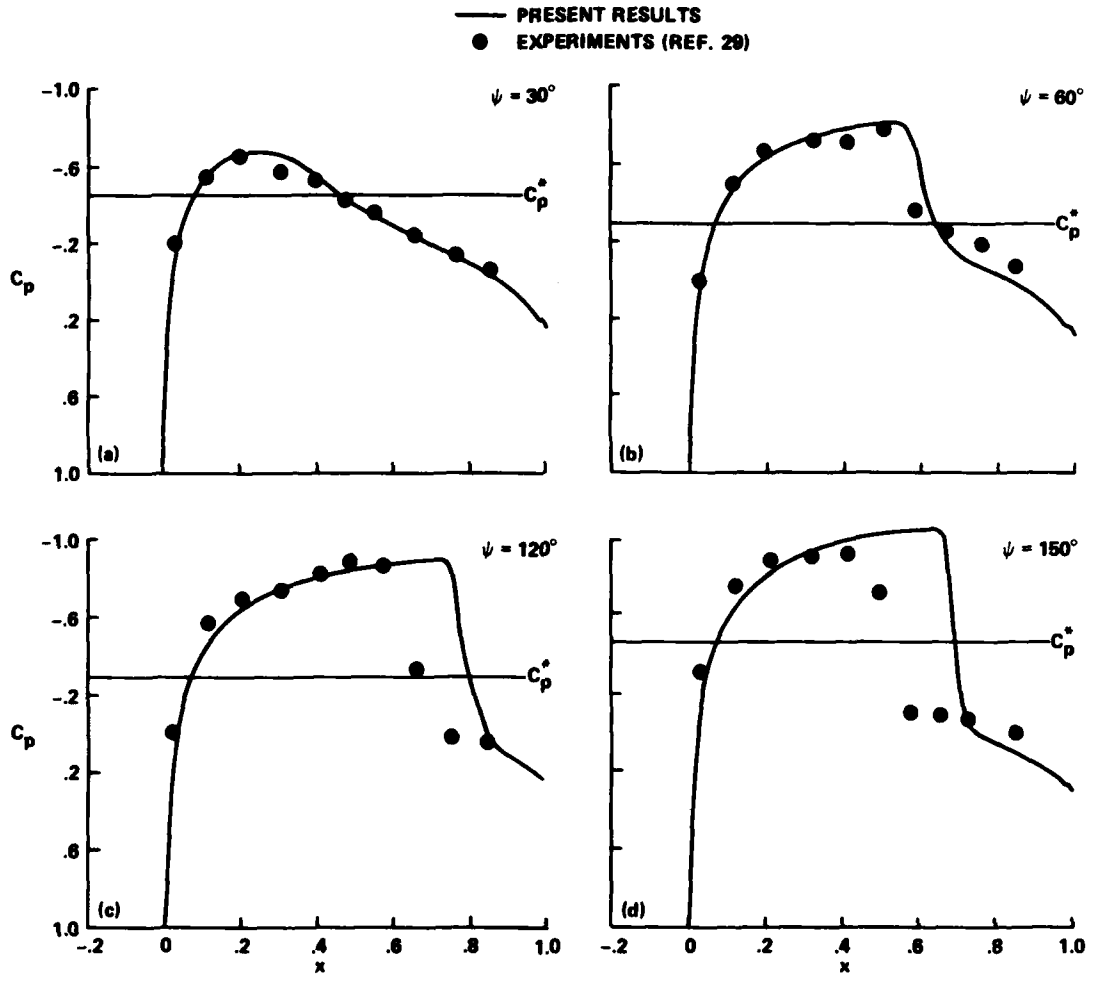

Fig. 9 Instantaneous surface-pressure distributions for the rotor-alone case: $M_T = 0.8$, $\mu = 0.2$, $r_B = 0.893$.

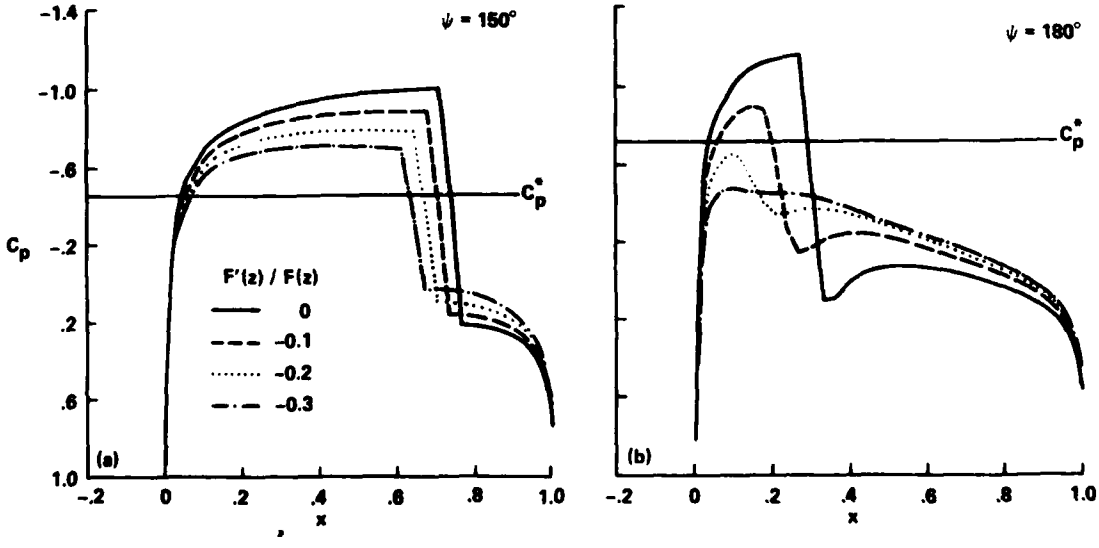

Fig. 10 Sensitivity of the numerical calculations to the three-dimensional correction factor B1: $M_T = 0.8$, $\mu = 0.2$, and $r_B = 0.893$.

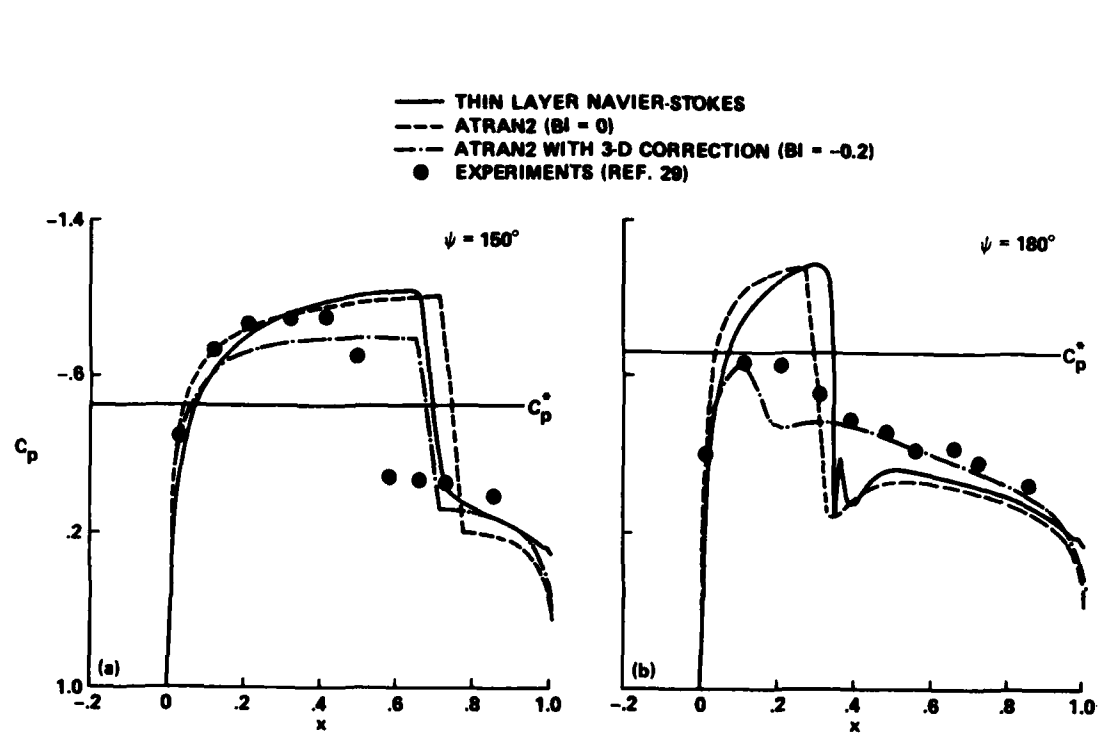

Fig. 11 Demonstration of the importance of the three-dimensional effect in the presence of shock waves: $M_T = 0.8$, $\mu = 0.2$, and $r_B = 0.893$.

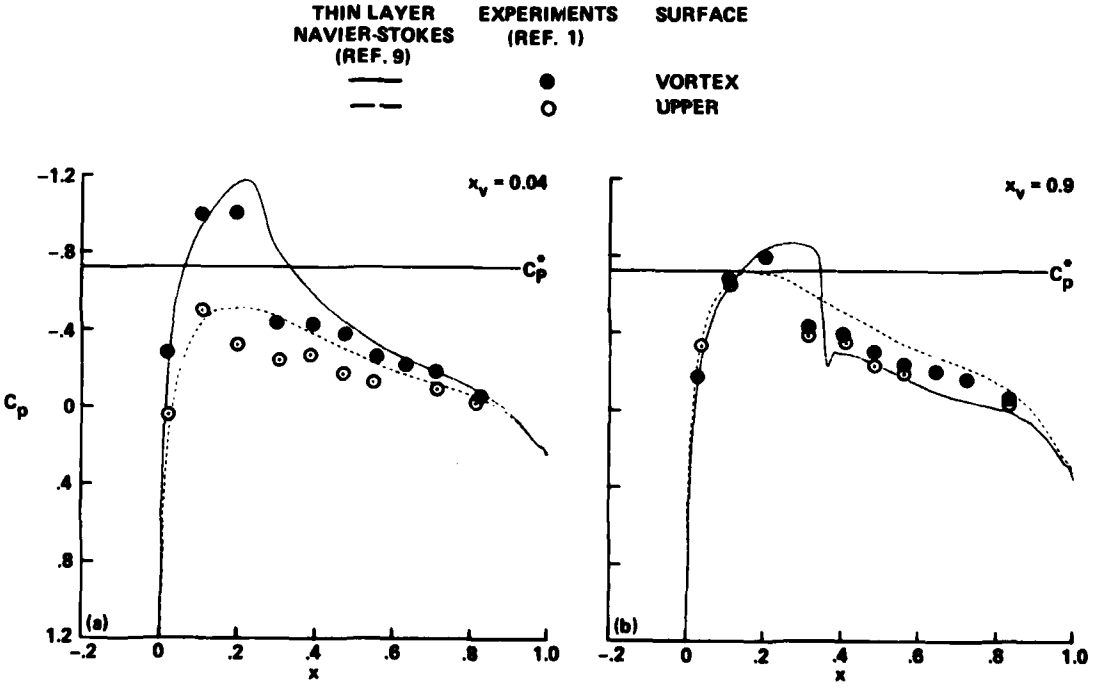

Fig. 12 Instantaneous surface-pressure distributions without considering unsteady time-lag effects: $M_r = 0.714$, $\hat{\Gamma} = 0.31$, $y_v = -0.4$.

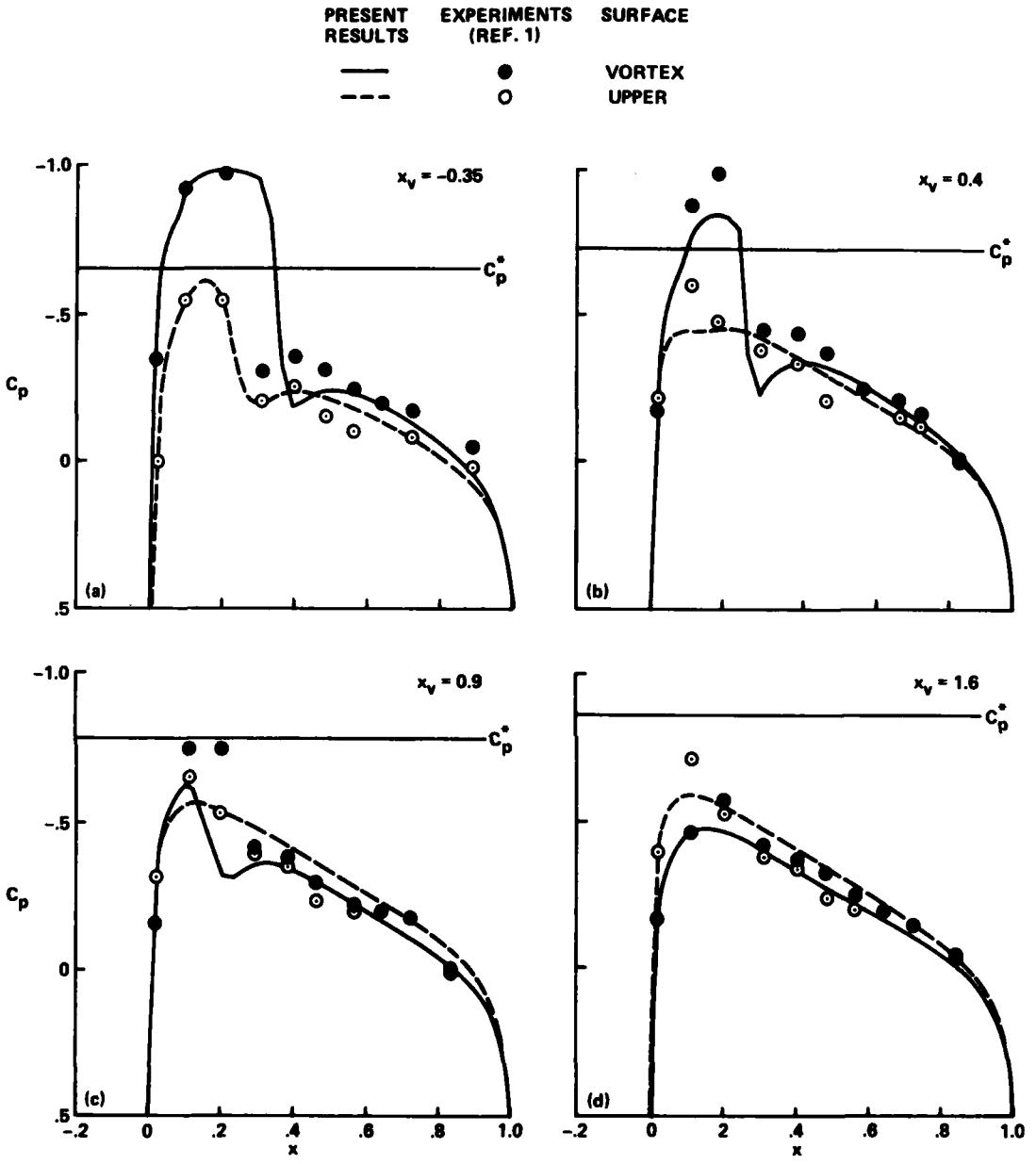

Fig. 13 Instantaneous surface-pressure distributions for the case of blade-vortex interaction, modified ATRAN2 solutions: $M_T = 0.8$, $\mu = 0.2$, $\hat{\Gamma} = 0.243$, and $y_v = -0.4$.

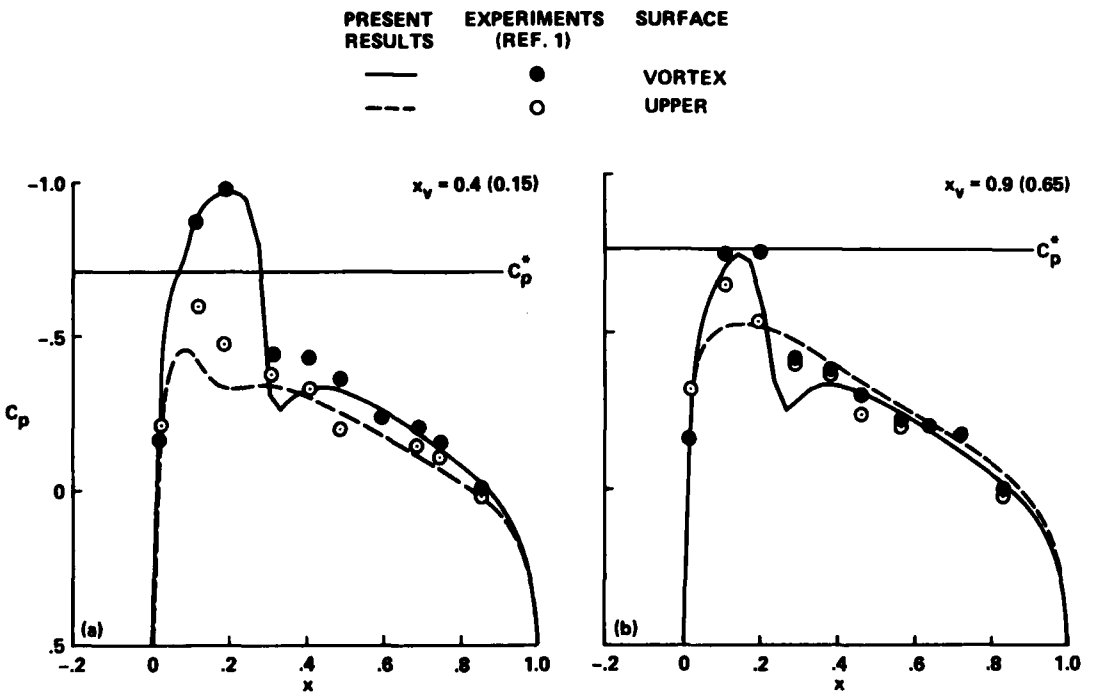

Fig. 14 Typical results for the case of Fig. 13 with calculations shifted by $x_v = -0.25$.

END

FILMED

12-85

DTIC